JOURNAL OF COMPUTATIONAL PHYSICS 98, 199–216 (1992)

Numerical Computation of 2D Sommerfeld Integrals—Decomposition of the Angular Integral

STEVEN L. DVORAK

Electromagnetics Laboratory, Department of Electrical and Computer Engineering, University of Arizona, Tucson, Arizona 85721

AND

EDWARD F. KUESTER

Electromagnetics Laboratory, Department of Electrical and Computer Engineering, Campus Box 425, University of Colorado, Boulder, Colorado 80309

Received April 6, 1990; revised December 13, 1990

Spectral domain techniques are frequently used in conjunction with Galerkin's method to obtain the current distribution on planar structures. When this technique is employed, a large percentage of the computation time is spent filling the impedance matrix. Therefore, it is important to develop accurate and efficient numerical techniques for the computation of the impedance elements, which can be written as two-dimensional (2D) Sommerfeld integrals. Once the current distribution has been found, then the near-zone electric field distribution can be obtained by computing another set of 2D Sommerfeld integrals. The computational efficiency of the 2D Sommerfeld integrals can be improved in two ways. The first method, which is discussed in this paper, involves finding a new way to compute the inner angular integral in the polar representation of these integrals. It turns out that the angular integral can be decomposed into a finite number of incomplete Lipschitz–Hankel integrals, which in turn can be calculated using series expansions. Therefore, the angular integral can be computed by summing a series instead of applying a standard numerical integration algorithm. This new technique is found to be more accurate and efficient when piecewise-sinusoidal basis functions are used to analyze a printed strip dipole antenna in a layered medium. The incomplete Lipschitz–Hankel integral representation for the angular integral is then used in another paper to develop a novel asymptotic extraction technique for the outer semi-infinite integral.

1. INTRODUCTION

The problem of finding the electromagnetic radiation from an electric current source in the presence of a stratified medium has been of interest for some time. In 1909, Sommerfeld solved the problem of a vertical electric Hertzian dipole over a homogeneous half-space [1]. Later, Hörschelman treated the case of a horizontal electric dipole in air [2], and Elias analyzed the vertical magnetic dipole in air [3]. Then in 1926, Sommerfeld treated all four cases of elementary Hertzian dipole sources in air [4].

There has been a substantial amount of work done on the Sommerfeld problem since 1926. For a good historical overview see [5]. Many of the authors who worked on the Sommerfeld problem obtained asymptotic expansions which hold for large observation distances from the source, or for large values of other parameters such as the relative permittivity of the earth [5–9]. These asymptotic expansions can be used to efficiently compute the far-fields and quasi-static fields. When the index of refraction is large, it is even possible to obtain asymptotic expansions for the near-fields.

While asymptotic expansions provide valuable physical insight into the Sommerfeld problem, they unfortunately cannot be used to compute the fields at all points in space for any given set of material parameters. However, with the introduction of high speed digital computers, it became possible to compute the Sommerfeld integrals at any point in space by using numerical techniques. Now, asymptotic techniques can be used in conjunction with numerical techniques to obtain an efficient algorithm for the computation of Sommerfeld integrals [10].

Green's functions for more complicated multilayer problems can also be calculated with the use of a computer [11–14]. Once the Green's function for a specific problem has been obtained, the fields can then be computed for any given distribution of current by convolving the Green's function with the source distribution. This operation can be written as

$$\mathbf{E}(\mathbf{x}) = \int_S \bar{\mathbf{G}}_e(\mathbf{x} - \mathbf{x}') \cdot \mathbf{J}(\mathbf{x}')\, ds', \tag{1}$$

where $\mathbf{x} = \mathbf{a}_x x + \mathbf{a}_y y + \mathbf{a}_z z$. When the current distribution is unknown, as is the case for a perfect conducting scatterer or

0021-9991/92 $3.00

antenna in a stratified medium, an electric field integral equation (EFIE) can be obtained by forcing the tangential component of the electric field to vanish at the surface of the perfect conducting body [15–21]. The method of moments (MOM) can then be used to reduce the EFIE to a set of linear equations which can be solved using standard matrix techniques [21–23]; thereby yielding an approximate distribution for the current on the body.

Before the matrix equation can be solved, the elements of the impedance matrix must be computed. A typical matrix elment can be written in the general form

$$Z_{mn} = \int_S \int_S \mathbf{w}_m(\mathbf{x}) \cdot \bar{\mathbf{G}}_e(\mathbf{x} - \mathbf{x}') \cdot \mathbf{f}_n(\mathbf{x}')\, ds\, ds', \qquad (2)$$

where $\mathbf{w}_m/\mathbf{f}_n$ is one of the chosen weighting/basis functions, respectively. This is classified as the spatial domain representation of the impedance elements. Since the evaluation of the Green's function involves a two-dimensional (2D) inverse Fourier transform, the computation of a typical matrix element will involve a sixfold integration. It is important to develop efficient techniques for the computation of (2), since the calculation of the elements in the impedance matrix usually requires a large percentage of the total computation time in a MOM problem. There are two different methods that are commonly used for this purpose.

In the first method, a polar transformation is applied to the Green's function, and then the angular integration is carried out in closed form—yielding Bessel functions of the first kind. The remaining semi-infinite integral can be classified as a one-dimensional (1D) Sommerfeld integral. Asymptotic extraction techniques, singularity extraction techniques, and other numerical techniques can then be applied to the 1D Sommerfeld integral [14, 17, 19, 24–31]. In [17, 25, 31], the authors point out that since the Green's function only depends on the distance between the source and field points, an interpolation scheme can be used in problems where the Green's function must be computed a large number of times. Once the Green's function can be efficiently computed, then the matric elements are obtained by using a four-dimensional numerical integration routine for the remaining finite integrals.

In the second method, the convolution theorem is used to rewrite the expressions for the electric field and the matrix elements as (see (1) and (2))

$$\begin{aligned} \mathbf{E}(\mathbf{x}) &= (2\pi)^2 \int_{-\infty}^{\infty} \int_{-\infty}^{\infty} \tilde{\tilde{\mathbf{G}}}_e(\alpha_1, \alpha_2, z - z') \\ &\quad \times \tilde{\mathbf{J}}(\alpha_1, \alpha_2, z')\, e^{-j(\alpha_1 x + \alpha_2 y)}\, d\alpha_1\, d\alpha_2 \\ Z_{mn} &= (2\pi)^4 \int_{-\infty}^{\infty} \int_{-\infty}^{\infty} \tilde{\tilde{\mathbf{w}}}_m(-\alpha_1, -\alpha_2, z) \\ &\quad \times \tilde{\tilde{\mathbf{G}}}_e(\alpha_1, \alpha_2, z - z')\, \tilde{\tilde{\mathbf{f}}}_n(\alpha_1, \alpha_2, z')\, d\alpha_1\, d\alpha_2. \end{aligned} \qquad (3)$$

If we choose basis and weighting functions whose Fourier transforms can be represented by combinations of algebraic functions and readily computed special functions, then the computation of a typical matrix element will only involve carrying out a 2D inverse Fourier transform. A polar transformation once again yields a Sommerfeld type integral, but this time the angular integral cannot be carried out in closed form. Therefore, this method involves the computation of 2D Sommerfeld integrals. The expressions in (3) are often referred to as the spectral domain representations for the electric field and the impedance elements. In [15, 32], the 2D Sommerfeld integrals are computed using a 2D numerical integration routine. Once again, asymptotic extraction techniques can be used to enhance the efficiency for the computation of the semi-infinite integral [33, 34].

Both of these methods have their advantages and disadvantages. If we assume that an interpolation table has already been constructed for the Green's function in the first method, then for each matrix element, a four-dimensional, definite integral must be computed using numerical techniques. On the other hand, a definite integral and a semi-infinite integral must be computed in the second method. The fact that the Green's function becomes singular as the distance between the source point and field point goes to zero presents some difficulties in the first method. In the second method, this problem shows up in the form of a slowly converging integral. Luckly, there are techniques which can be used to circumvent these difficulties [14, 26–30, 33, 34]. For a given problem, one method may be better suited than the other; but in general, both of these methods are important and need to be investigated further.

In two papers, we will develop accurate and efficient techniques for the computation of the 2D Sommerfeld integrals in (3) for the special case of piecewise-sinusoidal (PWS) basis and weighting functions (i.e., we will use Galerkin's method). In this paper, we will concentrate our efforts on developing techniques for the computation of the angular integral in the polar representation for the 2D Sommerfeld integrals. We will show that the angular integral can be represented in terms of incomplete Lipschitz–Hankel integrals (ILHIs). By using series expansions for the evaluation of these ILHIs, we can avoid using a numerical integration routine for the evaluation of the inner angular integral, thereby greatly improving the computational efficiency and accuracy for these 2D Sommerfeld integrals.

The problem of computing the outer semi-infinite integral is addressed in the second paper [35]. The decomposition of the angular integral in terms of ILHIs is used in [35] to develop a new asymptotic extraction technique (AET) for the outer semi-infinite integral in the 2D Sommerfeld integrals.

In order to demonstrate the usefulness of the techniques that are developed in these two papers, we will apply them to the problem of computing the driving-point input

impedance and the near-zone electric field distribution for a printed strip dipole antenna in a layered medium. These techniques are very general and can be applied to any planar structure whose current distribution can be adequately modeled using PWS basis functions.

We will make a number of references to [23, 36] in this paper, however, the material that is contained in these papers can also be found in [37].

2. EVALUATION OF THE 2D SOMMERFELD INTEGRALS

The printed strip dipole antenna, whose geometry is shown in Fig. 1, is assumed to be a perfectly conducting, infinitely thin piece of metal. The surface of the antenna is designated by S. In order to keep things as simple as possible, we will assume that the antenna is fed in the center by a sinusoidal delta-function gap voltage source and that the antenna is narrow enough so that the transverse component of the current can be neglected. The $e^{j\omega t}$ time dependence will be suppressed in this analysis. This structure was chosen because it is simple enough that it does not complicate the analysis, and at the same time it provides a good problem for comparison purposes.

The antenna is located in a general stratified medium. The inhomogeneous nature of this problem can be characterized by specifying a complex permittivity,

$$\varepsilon_{pq} = \varepsilon'_{pq} - \frac{j\sigma_{pq}}{\omega}, \tag{4}$$

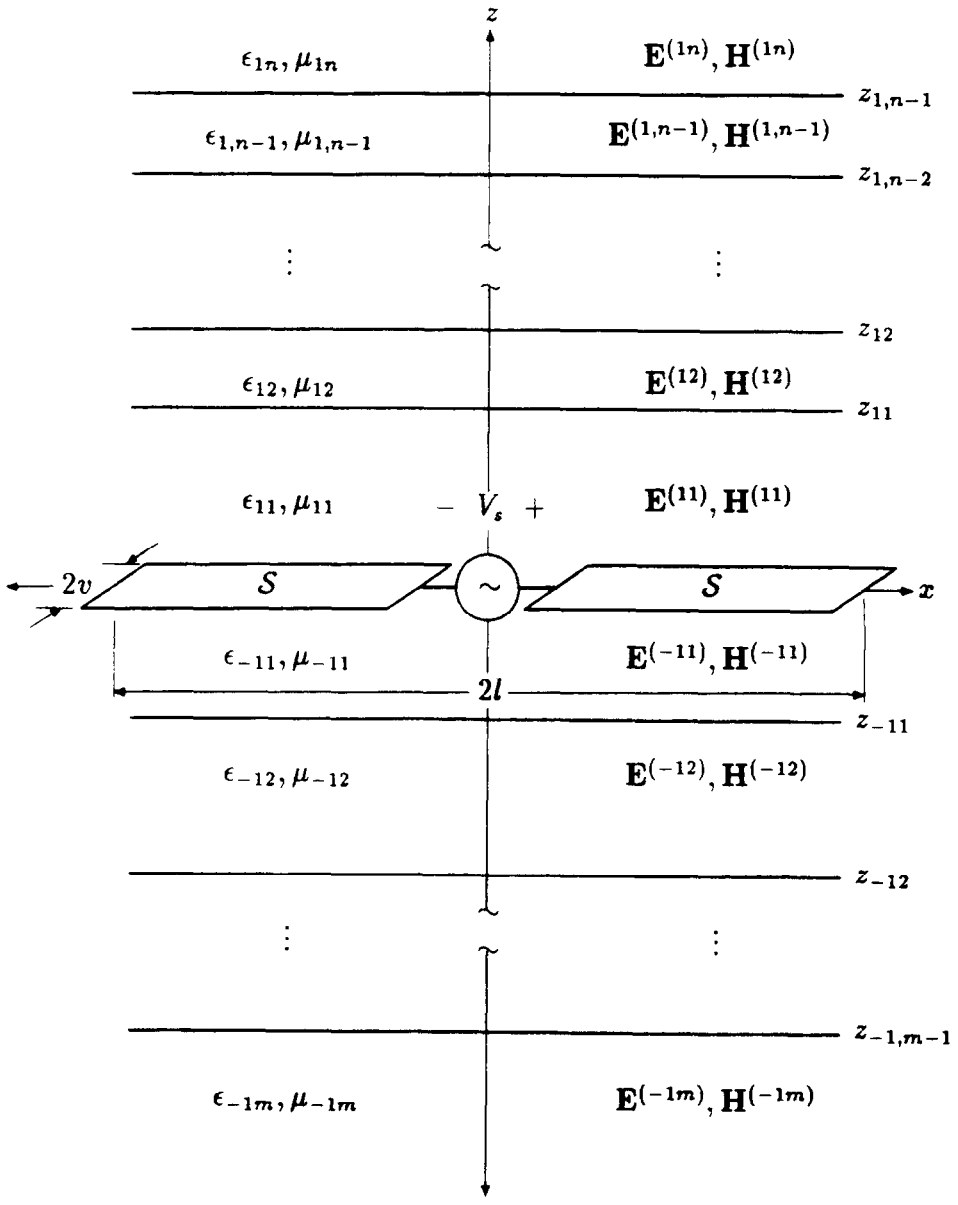

FIG. 1. Printed strip dipole antenna in a general stratified medium.

and a permeability, μ_{pq}, for each layer. The subscript pq denotes the qth layer in the positive z half-space when $p=1$, and the qth layer in the negative z half-space when $p=-1$.

The current on the antenna will be expanded in terms of PWS basis functions which are defined analytically as

$$J_x^{(n)}(x, y) = \left\{ \begin{array}{ll} \dfrac{\sin[k_A(d-|x-nd+l|)]}{2v\sin(k_A d)}; & |y|\leqslant v,\ |x-nd+l|\leqslant d \\ 0; & \text{otherwise} \end{array} \right\}, \tag{5}$$

where $d=2l/(N+1)$, N is the number of basis functions, and $k_A=\omega\sqrt{\mu_0\varepsilon_A}$. The value of k_A can be chosen arbitrarily; however, in some cases a judiciously chosen value for k_A can significantly improve the convergence of the solution. This basis function satisfies the boundary condition that requires the normal component of the current to vanish at the ends of the antenna and guarantees that the overall trial function will be continuous. It also has the advantage that the desired accuracy can often be obtained by using only one basis function when the antenna is near a resonance. This property is very useful—especially in array problems [38, 39]. The usefulness of the PWS basis function is demonstrated by the large number of authors that have chosen to use it in their work [15, 26, 28, 33, 34, 38–41].

We are interested in finding an efficient way to compute both the elements in an impedance matrix which results from a MOM formulation and the electric field which is due to a given current distribution on a printed strip dipole antenna in a layered medium. As was shown in [23], the computation of these quantities requires the evaluation of 2D Sommerfeld integrals. A 2D numerical integration routine can be used to compute these integrals, but it will require a large amount of CPU time. Therefore, it is desirable to find a more efficient computational method.

The 2D Sommerfeld integrals that need to be computed are

$$\begin{aligned} \mathbf{E}^{(pq)}(x, y, z) = {} & \frac{k_A}{2v\pi^2\sin(k_A d)} \sum_{n=1}^{N} I_n \int_0^\infty \{-\mathbf{a}_x\lambda \\ & \times \{[f_1^{(pq)}(\lambda, z) - f_2^{(pq)}(\lambda, z)]\, \mathscr{I}_1(k_A, \lambda, x \\ & + l - nd, y, (1, 0, 0, 0)) + f_2^{(pq)}(\lambda, z) \\ & \times \mathscr{I}_1(k_A, \lambda, x + l - nd, y, (1, 0, 1, 0))\} \\ & + \mathbf{a}_y\lambda[f_1^{(pq)}(\lambda, z) - f_2^{(pq)}(\lambda, z)] \\ & \times \mathscr{I}_1(k_A, \lambda, x + l - nd, y, (0, 1, 0, 0)) \\ & + \mathbf{a}_z\mathscr{I}_1(k_A, \lambda, x + l - nd, y, (1, 1, 1, 0)) \\ & \times f_3^{(pq)}(\lambda, z)\}\, \lambda\, d\lambda \end{aligned} \tag{6}$$

and

$$\begin{aligned} Z_{mn} = {} & \left[\frac{k_A}{v\pi\sin(k_A d)}\right]^2 \int_0^\infty \{[f_1^{(11)}(\lambda, 0) - f_2^{(11)}(\lambda, 0)] \\ & \times \mathscr{I}_1(k_A, \lambda, d(m-n), 0, (0, 0, 0, 1)) + f_2^{(11)}(\lambda, 0) \\ & \times \mathscr{I}_1(k_A, \lambda, d(m-n), 0, (0, 0, 1, 1))\}\, \lambda\, d\lambda, \end{aligned} \tag{7}$$

where the angular integral has the general form

$$\begin{aligned} & \mathscr{I}_1(k_A, \lambda, x, y, \mathbf{S}) \\ & = \int_{-\pi}^{\pi} \left\{\frac{[\cos(d\lambda\cos\theta) - \cos(k_A d)]\sin(v\lambda\sin\theta)}{k_A^2 - \lambda^2\cos^2\theta}\right\}^{S_4+1} \\ & \times \left\{\frac{\sin^{S_1}\theta\cos^{S_2}\theta}{1 - S_3^2\cos^2\theta}\right\} e^{-j\lambda(x\cos\theta + y\sin\theta)}\, d\theta \end{aligned} \tag{8}$$

and $\mathbf{S}=(S_1, S_2, S_3, S_4)$. The functions $f_1^{(pq)}(\lambda, z)$, $f_2^{(pq)}(\lambda, z)$, and $f_3^{(pq)}(\lambda, z)$ are similar in form to the expressions that are obtained in a transmission line analysis. Expressions for these functions are

$$\begin{aligned} f_1^{(pq)}(\lambda, z) &= \frac{\omega\mu_{pq}A_U^{(pq)}[e^{-jp\tau_{pq}z} + \Gamma_U^{(pq)}e^{jp\tau_{pq}z}]}{\lambda\sin\theta\tilde{\tilde{J}}_x^{(n)}(\lambda\cos\theta, \lambda\sin\theta)} \\ f_2^{(pq)}(\lambda, z) &= \frac{p\tau_{pq}A_V^{(pq)}[e^{-jp\tau_{pq}z} - \Gamma_V^{(pq)}e^{jp\tau_{pq}z}]}{\lambda\cos\theta\tilde{\tilde{J}}_x^{(n)}(\lambda\cos\theta, \lambda\sin\theta)} \\ f_3^{(pq)}(\lambda, z) &= \frac{\lambda^2 A_V^{(pq)}[e^{-jp\tau_{pq}z} + \Gamma_V^{(pq)}e^{jp\tau_{pq}z}]}{\lambda\cos\theta\tilde{\tilde{J}}_x^{(n)}(\lambda\cos\theta, \lambda\sin\theta)}. \end{aligned} \tag{9}$$

Since the fields must remain finite valued as $z\to\pm\infty$, we must restrict

$$\Im(\tau_{pq}) = \Im(\sqrt{k_{pq}^2 - \lambda^2}) \leqslant 0, \tag{10}$$

for $pq=1n$ and $pq=-1m$. For other values of pq, the above restriction is unnecessary; however, for the sake of consistency, we will use (10) for all values of pq.

Recurrence relations can be obtained for the amplitude and reflection coefficients by enforcing the boundary conditions at the source-free interfaces:

$$\begin{aligned} & A_U^{(pq)}\mu_{pq}e^{jp\tau_{pq}z_{pq}}[e^{-2jp\tau_{pq}z_{pq}} + \Gamma_U^{(pq)}] \\ & = A_U^{(p,q+1)}\mu_{p,q+1}e^{jp\tau_{p,q+1}z_{pq}}[e^{-2jp\tau_{p,q+1}z_{pq}} + \Gamma_U^{(p,q+1)}] \end{aligned} \tag{11}$$

$$\Gamma_U^{(pq)} = e^{-2jp\tau_{pq}z_{pq}} \times \frac{\left(\left[(e^{-2jp\tau_{p,q+1}z_{pq}} + \Gamma_U^{(p,q+1)}) - \frac{\mu_{pq}\tau_{p,q+1}}{\mu_{p,q+1}\tau_{pq}}(e^{-2jp\tau_{p,q+1}z_{pq}} - \Gamma_U^{(p,q+1)})\right]\right)}{\left(\left[(e^{-2jp\tau_{p,q+1}z_{pq}} + \Gamma_U^{(p,q+1)}) + \frac{\mu_{pq}\tau_{p,q+1}}{\mu_{p,q+1}\tau_{pq}}(e^{-2jp\tau_{p,q+1}z_{pq}} - \Gamma_U^{(p,q+1)})\right]\right)} \tag{12}$$

$$A_V^{(pq)}\varepsilon_{pq}e^{jp\tau_{pq}z_{pq}}[e^{-2jp\tau_{pq}z_{pq}} + \Gamma_V^{(pq)}] = A_V^{(p,q+1)}\varepsilon_{p,q+1}e^{jp\tau_{p,q+1}z_{pq}}[e^{-2jp\tau_{p,q+1}z_{pq}} + \Gamma_V^{(p,q+1)}] \tag{13}$$

$$\Gamma_V^{(pq)} = e^{-2jp\tau_{pq}z_{pq}} \times \frac{\left(\left[(e^{-2jp\tau_{p,q+1}z_{pq}} + \Gamma_V^{(p,q+1)}) - \frac{\varepsilon_{pq}\tau_{p,q+1}}{\varepsilon_{p,q+1}\tau_{pq}}(e^{-2jp\tau_{p,q+1}z_{pq}} - \Gamma_V^{(p,q+1)})\right]\right)}{\left(\left[(e^{-2jp\tau_{p,q+1}z_{pq}} + \Gamma_V^{(p,q+1)}) + \frac{\varepsilon_{pq}\tau_{p,q+1}}{\varepsilon_{p,q+1}\tau_{pq}}(e^{-2jp\tau_{p,q+1}z_{pq}} - \Gamma_V^{(p,q+1)})\right]\right)}. \tag{14}$$

If we assume that the only electric current sources are located at $z = 0$, then there will not be any waves coming in from $z = \pm\infty$. Therefore,

$$\Gamma_U^{(1n)} = \Gamma_V^{(1n)} = \Gamma_U^{(-1m)} = \Gamma_V^{(-1m)} = 0. \tag{15}$$

Since the reflection coefficients in the two semi-infinite regions are equal to zero, we can recursively compute the values of the reflection coefficients in the other layers by using (12) and (14). Also, reference to (11) and (13) shows that all of the amplitude coefficients in the upper/lower layers can be expressed in terms of the amplitude coefficients in the layers which are next to the sources (i.e., $A_{U,V}^{(11)}/A_{U,V}^{(-11)}$, respectively). Therefore, if we can find expressions for these amplitude coefficients, then the spectral domain fields will be uniquely determined.

Expressions for the amplitude coefficients in the layers adjacent to the antenna can be obtained by enforcing the boundary conditions at $z = 0$:

$$A_U^{(11)} = \left\{\frac{\tau_{11}(1-\Gamma_U^{(11)})}{\mu_{11}(1+\Gamma_U^{(11)})} + \frac{\tau_{-11}(1-\Gamma_U^{(-11)})}{\mu_{-11}(1+\Gamma_U^{(-11)})}\right\}^{-1} \times \frac{\lambda\sin\theta\tilde{\tilde{J}}_x - \lambda\cos\theta\tilde{\tilde{J}}_y}{\mu_{11}(1+\Gamma_U^{(11)})\lambda^2}$$
$$A_V^{(11)} = \left\{\frac{\varepsilon_{11}(1+\Gamma_V^{(11)})}{\tau_{11}(1-\Gamma_V^{(11)})} + \frac{\varepsilon_{-11}(1+\Gamma_V^{(-11)})}{\tau_{-11}(1-\Gamma_V^{(-11)})}\right\}^{-1} \times \frac{\lambda\cos\theta\tilde{\tilde{J}}_x + \lambda\sin\theta\tilde{\tilde{J}}_y}{\omega\tau_{11}(1-\Gamma_V^{(11)})\lambda^2}. \tag{16}$$

The 2D Sommerfeld integrals in (6) and (7), and the other results that are listed above, were obtained by using spectral domain techniques. See [23] for a detailed derivation of these equations.

This paper is devoted to finding an efficient way to compute the angular integrals in the 2D Sommerfeld integrals (8). The problem of the efficient computation of the outer integral is addressed in [35].

We have found that it is convenient to express (8) in terms of a new integral,

$$\mathcal{I}_3(k_A, \lambda, x, y, \mathbf{S}) = \int_{-\pi}^{\pi} \frac{\sin^{S_1}\theta\cos^{S_2}\theta}{(1-S_3^2\cos^2\theta)} \times \frac{e^{-j\lambda r(x,y)\cos[\theta-\theta_0(x,y)]}}{(k_A^2-\lambda^2\cos^2\theta)^{S_4+1}}\,d\theta, \tag{17}$$

where $r(x, y) = \sqrt{x^2+y^2}$ and $\theta_0(x, y) = \tan^{-1}(y/x)$. If we represent the trigonometric functions in the integrand of (8), which have trigonometric functions in their arguments, in terms of exponentials, and apply the identity

$$x\cos\theta + y\sin\theta = r\cos(\theta-\theta_0), \tag{18}$$

then it can be shown that (8) can be rewritten as

$$\mathcal{I}_1(k_A, \lambda, x, y, (S_1, S_2, S_3, 0)) = \frac{-1}{4j}\sum_{p=-1}^{1}[-2\cos(k_A d)]^{1-|p|} \times \sum_{q=-1}^{1} q\mathcal{I}_3(k_A, \lambda, x+pd, y+qv, (S_1, S_2, S_3, 0)), \tag{19}$$

$$\mathcal{I}_1(k_A, \lambda, x, y, (0, 0, S_3, 1)) = \frac{1}{16}\sum_{q=-1}^{1}[2-|q|](-1)^q \times \left\{[2+4\cos^2(k_A d)]\,\mathcal{I}_3(k_A, \lambda, x, y+q2v, \mathbf{S}) + \sum_{p=-2}^{2}{}'[-4\cos(k_A d)]^{2-|p|} \times \mathcal{I}_3(k_A, \lambda, x+pd, y+q2v, \mathbf{S})\right\}\Bigg|_{\mathbf{S}=(0,0,S_3,1)}, \tag{20}$$

where $\sum_p'$ means to sum over all p excluding $p = 0$.

If we can efficiently compute integrals which have the general form of (17), then we will be able to calculate the angular integrals in (6) and (7). In Appendix A, $\mathcal{I}_3$ is decomposed into a finite number of ILHIs, Bessel functions, and other elementary functions. The ILHIs that need to be computed have the general form

$$Je_0(a, z) = \int_0^z e^{-at} J_0(t)\, dt. \tag{21}$$

It is also shown in Appendix A that we can use the expression for $\hat{\mathcal{I}}_3$, which is given in Table III, in place of $\mathcal{I}_3$ and still obtain the correct result for $\mathcal{I}_1$ when S takes on one of the values in (26) or (27).

Now that we know how to express $\mathcal{I}_1$ in terms of a finite number of ILHIs, we must find an efficient way to compute these ILHIs. The ILHI, $Je_0(a, z)$, was studied extensively in [36]. An algorithm was presented in [36] which efficiently computes $Je_0(a, z)$ to a user defined number of significant digits (SD). This algorithm uses one of three different series expansions to compute $Je_0(a, z)$. The choice of which expansion to use depends on the parameters a, z, and SD. In Appendix B, we show how the results in [36] can be used to construct an efficient algorithm for the computation of $\hat{\mathcal{I}}_3$.

For the set of basis functions that we have chosen (see (5)), we will only need to compute $\mathcal{I}_1(k_A, \lambda, x, y, (0, 0, S_3, 1))$ for the special case of $y = 0$ (see (7)). If we had also chosen to segment the antenna in the y-direction, then y would have taken on non-zero values just as x does. At this point is is beneficial to look at some special cases, including the one which is discussed above. One interesting case occurs when $-y$ is substituted for y in (17). Using the change of variables, $\hat{\theta} = -\theta$, it is easy to show that

$$\mathcal{I}_3(k_A, \lambda, x, -y, \mathbf{S}) = (-1)^{S_1}\, \mathcal{I}_3(k_A, \lambda, x, y, \mathbf{S}). \tag{22}$$

Therefore, for the special case of $y = 0$, the terms in (20) for $q = -1$ are related to the terms for $q = 1$.

Similar simplifications arise for some special cases of x. This time, if we substitute $-x$ for x in (17), then we can use the change of variables, $\hat{\theta} = \pi - \theta$, to show that

$$\mathcal{I}_3(k_A, \lambda, -x, y, \mathbf{S}) = (-1)^{S_2}\, \mathcal{I}_3(k_A, \lambda, x, y, \mathbf{S}). \tag{23}$$

Therefore, further simplifications occur when computing $\mathcal{I}_1(k_A, \lambda, 0, 0, \mathbf{S})$. If we refer to (68) and (70), we find that these simplifications will also hold if $\mathcal{I}_3$ is replaced by $\hat{\mathcal{I}}_3$ in (20).

3. NUMERICAL EXAMPLES

To demonstrate the power of the techniques which have been developed in this paper, they will be applied in this section to the analysis of printed strip dipole antennas in layered media. The specific geometry that we are interested in is shown in Fig. 2. The presence of the perfectly conducting ground plane at $z = z_{-11}$ can be handled by finding the limiting cases for (12) and (14) when $\varepsilon_{-12} \to 1 - j\infty$. This procedure yields the following expressions for the reflection coefficients:

$$\begin{aligned} \Gamma_U^{(-11)} &= -e^{2j\tau_{-11}z_{-11}} \\ \Gamma_V^{(-11)} &= e^{2j\tau_{-11}z_{-11}}. \end{aligned} \tag{24}$$

We will only look at problems which include lossy dielectrics in this paper; therefore, a real-axis integration can be applied to the outer semi-infinite integrals in (6) and (7), since the poles and branch-points are located off of the real-axis. In problems where no losses are present, a real-axis integration can still be used provided that the pole extraction technique is employed [26]. We will use a version of the adaptive quadrature routine D01AKF [42] which has

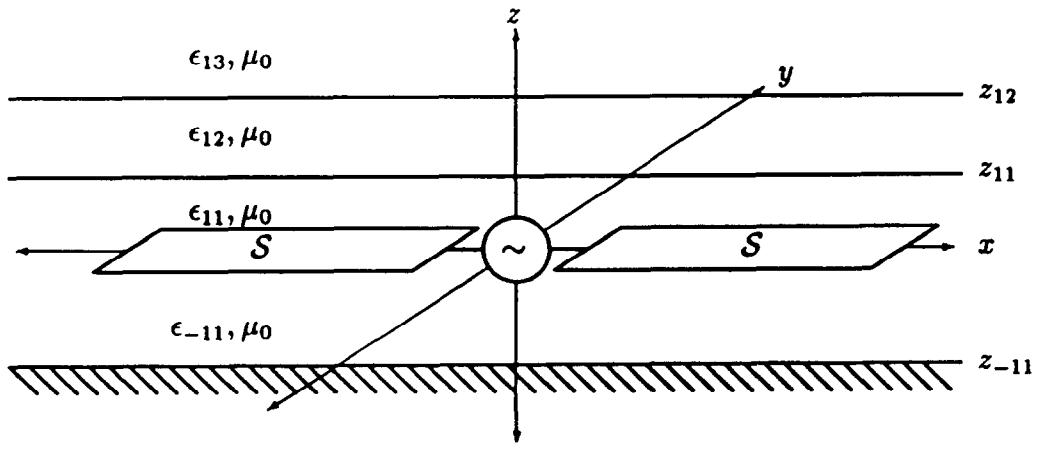

FIG. 2. Printed strip dipole antenna geometry used in the examples.

been modified to handle complex valued integrands to compute the outer integrals. These semi-infinite integrals are truncated at a suitable upper limit of integration, L. The inner angular integral (8) will be computed by using either the adaptive quadrature routine D01AKF or the decomposition in terms of ILHIs.

The impedance matrix is a symmetric Toeplitz matrix [43] for this problem. Therefore, we only need to compute Z_{m1} for $m = 1, 2, ..., N$, where N is the number of basis functions. The symmetric properties of the impedance matrix are used along with a number of other special properties to improve the computational efficiency for this problem (these techniques are discussed in detail in [23]).

We will first check our algorithm by comparing our results with the results in [34, Fig. 4]. In this example, we are interested in computing the input impedance of a printed strip dipole antenna on a grounded lossy substrate for different lengths of the antenna (λ_0 is the free space wavelength and should not be confused with the spectral variable λ). Since there are only two layers in this problem, we will set $z_{11} = z_{12} = 0$. The current on the dipole is expanded in terms of five PWS basis functions. The results are shown in Fig. 3. A visual comparison between Fig. 3 and [34, Fig. 4] confirms that the program is working properly. It should be noted that five PWS basis functions adequately model the current distribution when the antenna is operating near the first resonance; however, for longer antennas, more basis functions should probably be used to obtain accurate results. This example also shows that a real-axis integration can be used to compute the outer semi-infinite integral even when the losses in the problem are very small.

Now we will make a comparison between the two computational techniques for the inner angular integral (i.e., the decomposition in terms of ILHIs and the numerical integration routine D01AKF). In order to make this comparison, we will use both techniques to compute the current distribution on a printed strip dipole antenna which is intended for use as a hyperthermia applicator. A simplistic model in which the body tissue is represented as a layered medium will be used. The numerical examples were carried out on a Hewlett Packard 9000 series 300 computer.

We will analyze a hyperthermia applicator which has the same material and geometry parameters as those used in the example in [44]. However, we will use a printed strip dipole antenna, instead of a microstrip patch antenna, to excite the fields. An operating frequency of 915 MHz is used, and the antenna is assumed to be driven in the center by an idealized delta function gap voltage source. The antenna lies on a 0.5 cm thick grounded Rexolit substrate ($z_{-11} = -0.5$ cm and $\varepsilon_{-11} = 2.53\varepsilon_0$). A water bolus ($\varepsilon_{11} = 80\varepsilon_0$) is placed between the antenna and the muscle tissue in order to prevent overheating of the tissue which lies close to the antenna. Muscle tissue ($\varepsilon_{13} = (58 - j12)\,\varepsilon_0$) lies in the upper half-space which starts at $z_{11} = z_{12} = 0.5$ cm. All of the materials are nonmagnetic.

The only other parameters that need to be specified are the wavenumber for the basis functions, k_A, and the antenna dimensions (see Fig. 1). We will choose $\varepsilon_A = (\varepsilon_{11} + \varepsilon_{-11})/2 = 41.26\varepsilon_0$. Also, we will arbitrarily choose the width of the antenna to be $2v = 0.4$ cm, and we will use antenna lengths that correspond to the first and third resonances in this example. In Fig. 4, the input impedance is plotted versus the antenna length for the parameters given above. The results in this plot were obtained by expanding the current in terms of five PWS basis functions. From this plot we find that the first and third resonances occur when the antenna length is approximately equal to $2l = 2.34$ cm and $2l = 7.76$ cm, respectively.

In Table I, we have listed the amount of CPU time that is required to compute the elements in the impedance matrix to four significant digits of accuracy for a variable number of basis functions. The second column in this table shows

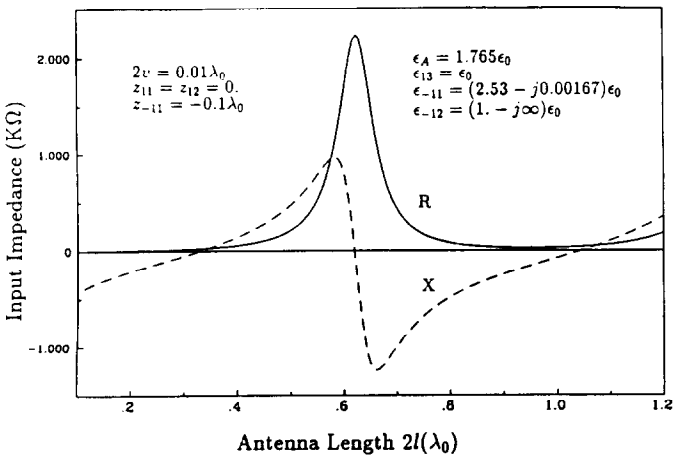

FIG. 3. Input impedance versus dipole antenna length.

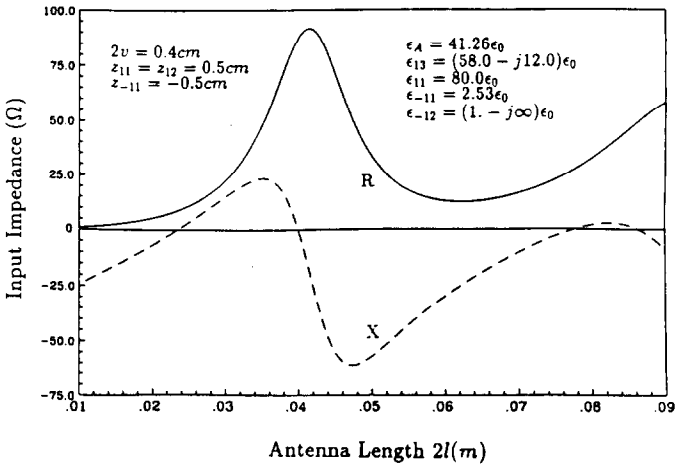

FIG. 4. Input impedance versus antenna length for the hyperthermia applicator.

TABLE I

Typical CPU Times for the Computation of the Elements in the Impedance Matrix for PWS Basis Functions

No. of basis functions	Upper limit L	Antenna length $2l = 2.34$ cm		$2l = 7.76$ cm	
		ILHIs	D01AKF	ILHIs	D01AKF
1	40,000	73.78 s	646.14 s	85.82 s	772.50 s
3	40,000	177.78	2510.02	257.20	‡
5	50,000	255.82	5087.02	590.62	‡
7	50,000	324.48	‡	820.22	‡
9	60,000	410.22	‡	1092.04	‡

where the outer semi-infinite integral was truncated. The values for L were obtained by trial and error. The amount of computation time required for the two different antenna lengths are shown in columns three and four, and five and six. In the columns headed by "ILHIs," the inner angular integral was computed using the decomposition technique. Numerical tests showed that requesting seven significant digits of accuracy from the expansions for the ILHIs assured the convergence of the outer numerical integration routine. The numerical integration routine D01AKF was applied in the columns headed by "D01AKF." It was found that requesting five significant digits was adequate for the numerical integration routine. When ‡ appears in a space, it means that the numerical integration routine could not produce the desired accuracy for the given inputs.

A comparison between columns three and four, or five and six shows that it is much more efficient to expand the angular integral in terms of ILHIs than to compute it using the quadrature routine D01AKF. Also, D01AKF failed to produce the desired accuracy of four significant digits in a number of cases. On the other hand, the decomposition in terms of ILHIs had no problems.

Table I also shows that a larger amount of computation time was required for the longer antenna than the shorter antenna. The reason for this is that the inner angular integral is more difficult to compute when the basis functions are widely separated.

Once the current distribution has been obtained on the antenna, then (6) can be used to obtain the associated electric field distribution. When analyzing hyperthermia applicators, it is important to find the heating distribution in the muscle tissue (i.e., $z \geqslant z_{11}$ in this example). The amount of heating that will occur in this simplified tissue model is proportional to $\sigma_{13} |\mathbf{E}^{(13)}(x, y, z)|^2$.

Now we will obtain heating patterns for the previously described hyperthermia applicator at the same values of z as those in Fig. 6 of [44]. We will use a dipole antenna whose length is $2l = 2.34$ cm and we will use five PWS basis functions for this analysis.

The electric field will be computed at a number of points in a grid. We will use a square grid that extends out to $|x_{\max}| = |y_{\max}| = 3l$, where $2l$ is the length of the dipole antenna. Due to the symmetry in this problem, we only have to compute the electric field in the first quadrant. If we compute 37 points in both the x and y directions, then the spacing between grid points will be (see (5))

$$\Delta x = \Delta y = \frac{3l}{36} = \frac{d}{4}. \tag{25}$$

This number was chosen so that we can apply the computational techniques that are discussed in [23]. The computed relative heating patterns are shown in Fig. 5. The peak values for these heating pattern are listed in the second column of Table II. The third column in Table II shows the relative values of the heating pattern on the z-axis.

The heating distribution that is obtained when using a dipole antenna differs significantly from the heating distribution for a microstrip antenna [44, Fig. 4]. The dipole heating distribution has two large peaks which are caused by the fringing fields at the ends of the dipole antenna. The fringing fields are only present in the near-field of the antenna. As the distance from the antenna increases, the contribution from the fringing fields becomes negligible.

The heating distribution for the microstrip applicator in [44] does not exhibit the fringing field effects that were observed with the dipole applicator. If we compare the results in Table II with [44, Fig. 4], we find that deeper penetration can be obtained by using the dipole applicator than the microstrip applicator. At a distance of 3 cm from

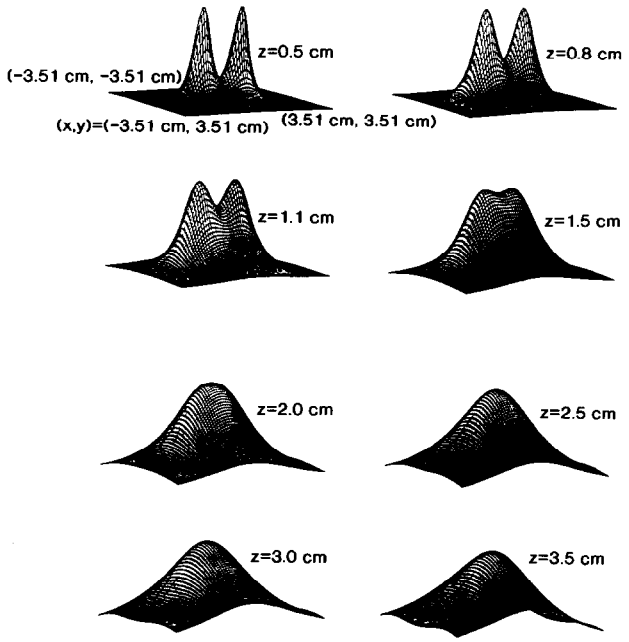

FIG. 5. Relative heating patterns for the hyperthermia applicator.

TABLE II

Relative Values for the Heating Distributions in Fig. 5

z (cm)	$\frac{\lvert\mathbf{E}(x, y, z)\rvert^2_{\max}}{\lvert\mathbf{E}(x, y, 0.5\text{ cm})\rvert^2_{\max}}$	$\frac{\lvert\mathbf{E}(0, 0, z)\rvert^2}{\lvert\mathbf{E}(x, y, 0.5\text{ cm})\rvert^2_{\max}}$
0.5	1.000	0.250
0.8	0.312	0.147
1.1	0.139	0.100
1.5	0.067	0.064
2.0	0.038	0.038
2.5	0.024	0.024
3.0	0.015	0.015
3.5	0.010	0.010

the microstrip applicator, the peak power absorption has fallen to $\frac{1}{256}$ of the power that was absorbed at a distance of 1.1 cm from the applicator. In the case of the dipole applicator, the peak power absorbed at $z = 3.0$ cm is nine times less than the power absorbed at $z = 1.1$ cm. Referring to Fig. 5 and [44, Fig. 6] we find that the heating distribution defocuses faster in the case of the microstrip applicator.

Actually, neither one of these antennas would make a very good applicator if it was used by itself. Referring to Table III we find that the magnitude of the peak electric field has decayed to e^{-1} of the maximum value that exists at the surface of the muscle tissue by the time it has penetrated only 0.6 cm into the muscle tissue. In comparison, a normally incident plane wave has a skin depth of 6.6 cm. Therefore, in order to obtain a useful applicator, an array of dipoles or microstrip antennas would have to be used.

The observations that we have made are only valid for the specific antennas that were analyzed. It may be possible to obtain a better applicator by operating one of the antennas in a different mode (i.e., change the antenna dimensions) or changing the applicator geometry.

We used two different methods to compute the heating distribution at $z = 0.5$ cm (see Fig. 5). In both methods the outer semi-infinite integral was computed using a version of D01AJF [42] which was modified to handle complex valued integrands. In order to obtain four significant digits of accuracy in the results, the numerical integration was carried out to $L = 1000.0$.

In the first method, the inner angular integral was expressed in terms of ILHIs. This method took 17122.3 CPU seconds to compute a 37×37 grid of points. This corresponds to an average of 12.51 CPU seconds per grid point.

In the second method, the inner angular integral was computed using the adaptive quadrature routine D01AJF. This method required 35096.4 CPU seconds, or 25.64 CPU seconds per point.

This example once again shows that expanding the angular integral in terms of ILHIs improves the efficiency for computing 2D Sommerfeld integrals. An even greater improvement in the efficiency would be obtained if the three components of the magnetic field were computed in addition to the three components of the electric field.

TABLE III

$\hat{\mathscr{I}}_3$ Decomposed into a Finite Number of ILHIs

$$\hat{\mathscr{I}}_3(k_A, \lambda, x, y, \mathbf{S})$$

$$= D_1\{\mathscr{I}_7(\lambda, x, y, S_1, 1) + (-1)^{S_1 - S_2}[\mathscr{I}_7(\lambda, x, y, S_1, 1)]^*\}$$
$$+ D_9\left\{\mathscr{I}_7\left(\lambda, x, y, S_1, \frac{k_A}{\lambda}\right) + (-1)^{S_1 - S_2}\left[\mathscr{I}_7\left(\lambda, x, y, S_1, \frac{k_A}{\lambda}\right)\right]^*\right\}$$
$$+ D_5\left\{\mathscr{I}_{10}\left(\lambda, x, y, \frac{k_A}{\lambda}\right) + \left[\mathscr{I}_{10}\left(\lambda, x, y, \frac{k_A}{\lambda}\right)\right]^*\right\}$$

$$D_1 = \frac{-(-S_3)^{1+S_2}}{2(k_A^2 S_3^2 - \lambda^2)^{1+S_4}}$$

$$D_5 = \frac{-S_4}{4k_A^2(k_A^2 S_3^2 - \lambda^2)}$$

$$D_9 = \frac{(-\lambda/k_A)^{1-S_2}}{2(k_A^2 S_3^2 - \lambda^2)}\left[\frac{3k_A^2 S_3^2 - \lambda^2}{2k_A^2(k_A^2 S_3^2 - \lambda^2)}\right]^{S_4} + \frac{\lambda k_A}{k_A^2 - \lambda^2} D_5$$

$$F_{\pm}(\theta_0, P) = \begin{cases} -P\cos\theta_0 \pm j\sin\theta_0\sqrt{P^2-1}; & P \geqslant 1 \\ -P\cos\theta_0 \pm \sin\theta_0\sqrt{1-P^2}; & 0 \leqslant P < 1 \end{cases}$$

$$\sqrt{1-F_{\pm}^2} = \begin{cases} \pm P\sin\theta_0 + j\cos\theta_0\sqrt{P^2-1}; & P \geqslant 1 \\ \pm P\sin\theta_0 + \cos\theta_0\sqrt{1-P^2}; & 0 \leqslant P < 1 \end{cases}$$

$$r(x, y) = \sqrt{x^2 + y^2}, \qquad \theta_0(x, y) = \tan^{-1}(y/x)$$

$$\mathscr{I}_7(\lambda, x, y, S_1, 1) = -2\pi j\{(-j\lambda y)^{1-S_1}\sin\theta_0 e^{j\lambda x} Je_0(j\cos\theta_0, \lambda r)$$
$$+ (1 - S_1)\lambda[xJ_0(\lambda r) + jrJ_1(\lambda r)]\}$$

$$\mathscr{I}_7(\lambda, x, y, S_1, P)$$
$$= -\pi j(j\sqrt{P^2-1})^{S_1-1}\{e^{-j\lambda F_+ r}\sqrt{1-F_+^2}\, Je_0(-jF_+, \lambda r)$$
$$+ (-1)^{S_1} e^{-j\lambda F_- r}\sqrt{1-F_-^2}\, Je_0(-jF_-, \lambda r)\}$$

$$\mathscr{I}_{10}(\lambda, x, y, P)$$
$$= \frac{\pi\lambda r}{(P^2-1)}\{e^{-j\lambda F_+ r}(1-F_+^2)\, Je_0(-jF_+, \lambda r)$$
$$+ e^{-j\lambda F_- r}(1-F_-^2)\, Je_0(-jF_-, \lambda r) - 2[J_1(\lambda r) - jP\cos\theta_0 J_0(\lambda r)]\}$$

4. CONCLUSION

We have demonstrated in this paper that the angular integral, in the 2D Sommerfeld integral associated with PWS basis functions, can be represented in terms of a finite number of ILHIs. We have also shown that representing the angular integral in this manner provides a more accurate and efficient method for computing the angular integral than using a standard numerical integration routine. Furthermore, it is shown in [35] that the expansion of the

angular integral in terms of ILHIs can be used to develop a novel asymptotic extraction technique for the outer semi-infinite integral. This asymptotic extraction technique provides further improvements in both the accuracy and efficiency.

The techniques which have been developed in this paper are not restricted to PWS basis functions. They can be used with any basis functions which result in angular integrals which have the general form (8). This includes entire domain [37, Chap. 8], rooftop [45], pulse, and traveling wave basis functions.

APPENDIX A: DECOMPOSITION OF $\mathcal{I}_3$ INTO A FINITE NUMBER OF ILHIS

A.1. *Introduction*

In this appendix, we will decompose (17) into a series of ILHIs. This integral will exhibit a different behavior for each different value of S. If we are interested in computing an impedance element, then we will need to compute $\mathcal{I}_3$ for (see (7))

$$\mathbf{S}=\begin{Bmatrix}(0,0,0,1)\\(0,0,1,1)\end{Bmatrix}. \tag{26}$$

On the other hand, if we are interested in computing the electric field, then (see (6))

$$\mathbf{S}=\begin{Bmatrix}(1,0,0,0)\\(1,0,1,0)\\(0,1,0,0)\\(1,1,1,0)\end{Bmatrix}. \tag{27}$$

A.2. *Partial Fraction Decomposition*

We will first define two new integrals,

$$\mathcal{I}_4(\lambda, x, y, S_1, P)=\int_{-\pi}^{\pi}\frac{\sin^{S_1}\theta e^{-j\lambda r(x,y)\cos[\theta-\theta_0(x,y)]}}{\cos\theta+P}\,d\theta \tag{28}$$

$$\mathcal{I}_5(\lambda, x, y, P)=\int_{-\pi}^{\pi}\frac{e^{-j\lambda r(x,y)\cos[\theta-\theta_0(x,y)]}}{(\cos\theta+P)^2}\,d\theta. \tag{29}$$

By making the change of variables, $\hat{\theta}=\theta-\pi$, it is easy to show that

$$\begin{aligned}\mathcal{I}_4(\lambda, x, y, S_1, -P)&=-(-1)^{S_1}[\mathcal{I}_4(\lambda, x, y, S_1, P)]^*\\ \mathcal{I}_5(\lambda, x, y, -P)&=[\mathcal{I}_5(\lambda, x, y, P)]^*.\end{aligned} \tag{30}$$

If we apply a partial fraction expansion to the integrand of (17) and use the results in (30), then we can show that

$$\begin{aligned}&\mathcal{I}_3(k_A, \lambda, x, y, \mathbf{S})\\ &\quad=D_1[\mathcal{I}_4(\lambda, x, y, S_1, 1)+(-1)^{S_1-S_2}\\ &\qquad\times[\mathcal{I}_4(\lambda, x, y, S_1, 1)]^*]\\ &\qquad+D_3\left[\mathcal{I}_4\left(\lambda, x, y, S_1, \frac{k_A}{\lambda}\right)+(-1)^{S_1-S_2}\right.\\ &\qquad\left.\times\left[\mathcal{I}_4\left(\lambda, x, y, S_1, \frac{k_A}{\lambda}\right)\right]^*\right]\\ &\qquad+D_5\left[\mathcal{I}_5\left(\lambda, x, y, \frac{k_A}{\lambda}\right)\right.\\ &\qquad\left.+\left[\mathcal{I}_5\left(\lambda, x, y, \frac{k_A}{\lambda}\right)\right]^*\right],\end{aligned} \tag{31}$$

where

$$\begin{aligned}D_1&=\frac{-(-S_3)^{1+S_2}}{2(k_A^2S_3^2-\lambda^2)^{1+S_4}}\\ D_3&=\frac{(-\lambda/k_A)^{1-S_2}}{2(k_A^2S_3^2-\lambda^2)}\left[\frac{3k_A^2S_3^2-\lambda^2}{2k_A^2(k_A^2S_3^2-\lambda^2)}\right]^{S_4}\\ D_5&=\frac{-S_4}{4k_A^2(k_A^2S_3^2-\lambda^2)}.\end{aligned} \tag{32}$$

This equation holds for all the values of S that are shown in (26) and (27).

Now we need to evaluate integrals which are of the form given in (28) and (29). We will first concentrate on evaluating $\mathcal{I}_4$. In order to simplify the exponential factor in (28), we make the change of variables, $\hat{\theta}=\theta-\theta_0$ and apply the addition formulas to the resulting trigonometric functions, thereby obtaining

$$\begin{aligned}\mathcal{I}_4(\lambda, x, y, S_1, P)=\int_{-\pi}^{\pi}&\frac{[\sin\hat{\theta}\cos\theta_0+\cos\hat{\theta}\sin\theta_0]^{S_1}}{[\cos\hat{\theta}\cos\theta_0-\sin\hat{\theta}\sin\theta_0+P]}\\ &\times e^{-j\lambda r\cos\hat{\theta}}\,d\hat{\theta}.\end{aligned} \tag{33}$$

Since the variable of integration in (28) ranges over one full period of the integrand, the only restriction that was placed on chosing the limits of integration in (33) was that they also allow for integration over one full period.

At this point it is beneficial to rearrange the integrand of (33) in such a way that $\hat{\theta}$ only appears in the form of $\cos\hat{\theta}$ in the denominator. This can be accomplished by multiplying the numerator and denominator by $(\cos\hat{\theta}\cos\theta_0+P+\sin\hat{\theta}\sin\theta_0)$. After multiplying out the numerator, the integral can be simplified by neglecting any odd functions of

$\hat{\theta}$ which appear in the numerator since they will integrate to zero. Two cases are possible since $S_1 = 0$ or $S_1 = 1$:

$$\mathcal{I}_4(\lambda, x, y, 0, P) = \int_{-\pi}^{\pi} \frac{[P + \cos\theta_0 \cos\hat{\theta}]}{[P^2 - \sin^2\theta_0 + 2P\cos\hat{\theta}\cos\theta_0 + \cos^2\hat{\theta}]} \times e^{-j\lambda r\cos\hat{\theta}}\, d\hat{\theta}$$

$$\mathcal{I}_4(\lambda, x, y, 1, P) = \sin\theta_0 \int_{-\pi}^{\pi} \frac{[P\cos\hat{\theta} + \cos\theta_0]}{[P^2 - \sin^2\theta_0 + 2P\cos\hat{\theta}\cos\theta_0 + \cos^2\hat{\theta}]} \times e^{-j\lambda r\cos\hat{\theta}}\, d\hat{\theta}. \tag{34}$$

The denominators in (34) can be factorized and then a second partial fraction expansion can be used to show that

$$\mathcal{I}_4(\lambda, x, y, S_1, P) = D_7 \mathcal{I}_6(\lambda, x, y, F_+) + D_8 \mathcal{I}_6(\lambda, x, y, F_-), \tag{35}$$

where an expression for $F_\pm$ is given in Table III, and

$$\mathcal{I}_6(\lambda, x, y, F_\pm) = \int_{-\pi}^{\pi} \frac{e^{-j\lambda r\cos\theta}}{\cos\theta - F_\pm(\theta_0, P)}\, d\theta, \tag{36}$$

$$\left.\begin{aligned} D_7 &= \left[\frac{\cos\theta_0\sqrt{P^2-1} - jP\sin\theta_0}{2\sqrt{P^2-1}}\right][j\sqrt{P^2-1}]^{S_1} \\ D_8 &= \left[\frac{\cos\theta_0\sqrt{P^2-1} + jP\sin\theta_0}{2\sqrt{P^2-1}}\right][-j\sqrt{P^2-1}]^{S_1} \end{aligned}\right\}; \quad P \geq 1. \tag{37}$$

A.3. *Representation in Terms of ILHIs*

The integral, $\mathcal{I}_6$, can now be rewritten in terms of special functions. Using the integral representation of the Bessel function, it can be shown that $\mathcal{I}_6$ satisfies the first-order, non-homogeneous, ordinary differential equation:

$$\frac{d\mathcal{I}_6}{dr} + j\lambda F_\pm \mathcal{I}_6 = -2\pi j\lambda J_0(\lambda r). \tag{38}$$

The solution of (38) is given by

$$\mathcal{I}_6(\lambda, x, y, F_\pm) = -2\pi j e^{-j\lambda F_\pm r} \int_{\delta}^{\lambda r} e^{jF_\pm t} J_0(t)\, dt, \tag{39}$$

where δ is a constant which is yet to be determined. If we replace the Bessel function by its integral representation, interchange the order of integration, and carry out the resulting integral, we find that

$$\mathcal{I}_6(\lambda, x, y, F_\pm) = e^{-j\lambda F_\pm r} \int_{-\pi}^{\pi} \frac{e^{jt(F_\pm - \cos\theta)}}{\cos\theta - F_\pm}\Bigg|_{\delta}^{\lambda r} d\theta. \tag{40}$$

By comparing (36) with (40), we find that δ can be defined as

$$\delta = \left\{\begin{matrix} \infty; \Re(jF_\pm) \leq 0 \\ -\infty; \Re(jF_\pm) > 0 \end{matrix}\right\}. \tag{41}$$

In addition, reference to (21) shows that (39) can be rewritten in terms of ILHIs:

$$\mathcal{I}_6(\lambda, x, y, F_\pm) = -2\pi j e^{-j\lambda F_\pm r}\{Je_0(-jF_\pm, \lambda r) - Je_0(-jF_\pm, \delta)\}. \tag{42}$$

ILHIs were studied in great detail in [36]. We will use many of the results that were obtained in [36] in this appendix.

A.4. $\mathcal{I}_3$ *for* $0 \leq \lambda < k_A$

If we refer back to (28) and (29), we find that there are apparent singularities in the denominators of the two integrands when $0 \leq P \leq 1$. On the other hand, the apparent singularities in the denominator of (8) are actually removable singularities for the values of S given in (26) and (27). Since $\mathcal{I}_1$ can be decomposed into a finite number of integrals which have the form of $\mathcal{I}_4$ and $\mathcal{I}_5$, it must be possible to remove the apparent singularities when the integrals are added together.

When $P > 1$, there are no singularities, so no problems exist. Therefore, we will first deal with this case, and later we will use analytic continuation to obtain a solution which is valid when $0 \leq P < 1$. Using [36, (45)–(47), (49)], it can be shown that

$$Je_0(-jF_\pm, \delta) = 1/\sqrt{1 - F_\pm^2}, \tag{43}$$

where the branch cut for the square root is defined by

$$\begin{aligned} &\Re(\sqrt{1-F_\pm^2}) \geq 0; \quad \Re(jF_\pm) \leq 0, \\ &\Re(\sqrt{1-F_\pm^2}) < 0; \quad \Re(jF_\pm) > 0. \end{aligned} \tag{44}$$

Using the definition for $F_\pm$ in Table III, we find that

$$\left.\begin{aligned} \Re(jF_\pm) &= \mp\sin\theta_0\sqrt{P^2-1} \\ 1 - F_\pm^2 &= (\pm P\sin\theta_0 + j\cos\theta_0\sqrt{P^2-1})^2 \end{aligned}\right\}; \quad P > 1. \tag{45}$$

In order to satisfy the condition in (44) when $P > 1$, the branch cut for $\sqrt{1-F_\pm^2}$ must be defined as in Table III. Referring to (37), we find that the expressions for D_7 and D_8

can be simplified by applying the expression for $\sqrt{1-F_{\pm}^2}$ in Table III:

$$D_7 = \frac{\sqrt{1-F_+^2}}{2j\sqrt{P^2-1}}\left[j\sqrt{P^2-1}\right]^{S_1}$$
$$D_8 = \frac{\sqrt{1-F_-^2}}{2j\sqrt{P^2-1}}\left[-j\sqrt{P^2-1}\right]^{S_1}. \tag{46}$$

Finally, combining the results in (35), (42), (43), and (46), yields

$$\mathcal{I}_4(\lambda, x, y, S_1, P) = \mathcal{I}_7(\lambda, x, y, S_1, P) + \mathcal{I}_8(\lambda, x, y, S_1, P), \tag{47}$$

where an expression for $\mathcal{I}_7$ is given in Table III, and

$$\mathcal{I}_8(\lambda, x, y, S_1, P) = \pi j\left(j\sqrt{P^2-1}\right)^{S_1-1} \times \left\{e^{-j\lambda F_+ r} + (-1)^{S_1} e^{-j\lambda F_- r}\right\}. \tag{48}$$

Writing $\mathcal{I}_4$ in this way simplifies the analysis since, as is shown below, the term $\mathcal{I}_8$ will cancel with other terms when the pieces are recombined to yield $\mathcal{I}_1$. First, it is easy to show that

$$\mathcal{I}_8(\lambda, x+d, y, S_1, P) + \mathcal{I}_8(\lambda, x-d, y, S_1, P) - 2\cos(k_A d)\,\mathcal{I}_8(\lambda, x, y, S_1, P) = 0, \tag{49}$$

when $S_4 = 0$ and $P = k_A/\lambda$. Since $\mathcal{I}_8$ only appears in linear combinations which have the form given in (49) (see (19), (31), and (47)), we can cancel $\mathcal{I}_8$ from (47) and still obtain the correct result for $\mathcal{I}_1$ when $S_4 = 0$ and $P > 1$. Likewise, it can also be shown that

$$\begin{aligned}(2+4\cos^2(k_A d))\,\mathcal{I}_8(\lambda, x, y, S_1, P) - 4\cos(k_A d) \\ \times\left[\mathcal{I}_8(\lambda, x+d, y, S_1, P) + \mathcal{I}_8(\lambda, x-d, y, S_1, P)\right] \\ + \mathcal{I}_8(\lambda, x+2d, y, S_1, P) \\ + \mathcal{I}_8(\lambda, x-2d, y, S_1, P) = 0,\end{aligned} \tag{50}$$

when $S_4 = 1$ and $P = k_A/\lambda$. Therefore, we can once again cancel $\mathcal{I}_8$ in (47) and still obtain the correct result for $\mathcal{I}_1$ when all of the pieces are added together (see (20), (31), and (47)). Therefore, we can define

$$\begin{aligned}\hat{\mathcal{I}}_3(k_A, \lambda, x, y, \mathbf{S}) &= D_1\left[\mathcal{I}_7(\lambda, x, y, S_1, 1) + (-1)^{S_1-S_2} \times \left[\mathcal{I}_7(\lambda, x, y, S_1, 1)\right]^*\right] \\ &+ D_3\left[\mathcal{I}_7\left(\lambda, x, y, S_1, \frac{k_A}{\lambda}\right) + (-1)^{S_1-S_2} \times\left[\mathcal{I}_7\left(\lambda, x, y, S_1, \frac{k_A}{\lambda}\right)\right]^*\right] \\ &+ D_5\left[\mathcal{I}_5\left(\lambda, x, y, \frac{k_A}{\lambda}\right) + \left[\mathcal{I}_5\left(\lambda, x, y, \frac{k_A}{\lambda}\right)\right]^*\right],\end{aligned} \tag{51}$$

where the hat on $\mathcal{I}_3$ serves as a reminder that this expression will give an incorrect value for (17), but it will yield the correct results for the integral of interest, $\mathcal{I}_1$, when all of the pieces are added together.

In order to evaluate (51) for $0 \leqslant \lambda < k_A$, we need to find an expression for $\mathcal{I}_7(\lambda, x, y, S_1, 1)$. When $S_1 = 1$, it is easy to show that

$$\mathcal{I}_7(\lambda, x, y, 1, 1) = -2\pi j \sin\theta_0 e^{j\lambda x} Je_0(j\cos\theta_0, \lambda r), \tag{52}$$

where we have made use of the results in Table III. This case was easy to handle since the singularity in $\mathcal{I}_4(\lambda, x, y, 1, 1)$ is a removable singularity (see (28)). On the other hand, it is more difficult to find $\mathcal{I}_7(\lambda, x, y, 0, 1)$, since $\mathcal{I}_4(\lambda, x, y, 0, P)$ has a non-removable singularity at $P = 1$. As was previously mentioned, the singularity at $P = 1$ is a removable singularity in (8); therefore, it must also be possible to remove this singularity by adding the pieces which $\mathcal{I}_1$ was decomposed into back together.

As it turns out, the singular part of $\mathcal{I}_4(\lambda, x, y, 0, 1)$ is contained totally in $\mathcal{I}_8(\lambda, x, y, 0, 1)$. We have previously shown that the term $\mathcal{I}_8$ will cancel with other terms when all of the pieces are added together to obtain $\mathcal{I}_1$; therefore, we will not have to deal with this singular piece. The other term in (47) only contains a removable singularity. Therefore, we can obtain an expression for $\mathcal{I}_7(\lambda, x, y, 0, 1)$ by removing this singularity. If we substitute the expressions for $F_{\pm}$ and $\sqrt{1-F_{\pm}^2}$ into $\mathcal{I}_7$, then we can use (21) to show that

$$\begin{aligned}\mathcal{I}_7(\lambda, x, y, 0, 1) &= \lim_{P\to 1}\frac{2\pi}{\sqrt{P^2-1}}\int_0^{\lambda r} e^{-jP\cos\theta_0(t-\lambda r)} \\ &\times\left\{P\sin\theta_0 \sinh\left[\sin\theta_0\sqrt{P^2-1}\,(t-\lambda r)\right]\right. \\ &\left. - j\cos\theta_0\sqrt{P^2-1}\cosh\left[\sin\theta_0\sqrt{P^2-1}\right.\right. \\ &\left.\left.\times(t-\lambda r)\right]\right\} J_0(t)\,dt.\end{aligned} \tag{53}$$

Expanding the hyperbolic functions in power series expansions, yields

$$\mathcal{I}_7(\lambda, x, y, 0, 1) = 2\pi \left\{ -e^{j\lambda x} Je_0(j\cos\theta_0, \lambda r) \times [\lambda r \sin^2\theta_0 + j\cos\theta_0] + \sin^2\theta_0 \int_0^{\lambda r} e^{-j\cos\theta_0 (t-\lambda r)} t J_0(t)\, dt \right\}. \quad (54)$$

In order to simplify this equation, we need to find an expression for integrals which have the form

$$\mathcal{I}_9(a, z) = e^{az} \int_0^z e^{-at} t J_0(t)\, dt. \quad (55)$$

After integrating by parts, with $u = e^{-at}$ and $dv = tJ_0(t)\, dt$, we find that

$$\mathcal{I}_9(a, z) = zJ_1(z) + ae^{az} Je_1(a, z). \quad (56)$$

Using [36, (9), (12)], we can rewrite (56) as

$$\mathcal{I}_9(a, z) = \frac{1}{(a^2+1)} \{ ae^{az} Je_0(a, z) + zJ_1(z) - azJ_0(z) \}. \quad (57)$$

Now we can find an expression for (54) by applying (57)

$$\mathcal{I}_7(\lambda, x, y, 0, 1) = -2\pi\lambda \{ y \sin\theta_0 e^{j\lambda x} Je_0(j\cos\theta_0, \lambda r) + jxJ_0(\lambda r) - rJ_1(\lambda r) \}. \quad (58)$$

We can combine the results in (52) and (58) to obtain the general form of $\mathcal{I}_7$ which is given in Table III.

Before we can evaluate (51) for $\lambda < k_A$, we still need to find an expression for (29). Using the definitions in (28) and (29), it is easy to show that

$$\mathcal{I}_5(\lambda, x, y, P) = -\frac{d\mathcal{I}_4(\lambda, x, y, 0, P)}{dP}. \quad (59)$$

Therefore, we can obtain an expression for $\mathcal{I}_5$ by differentiating (47) with respect to P.

Before actually carrying out the differentiation, we will derive some intermediate results. Using the results in Table III, it can be shown that

$$\frac{dF_\pm}{dP} = \frac{j\sqrt{1-F_\pm^2}}{\sqrt{P^2-1}}; \qquad P > 1. \quad (60)$$

It can also be shown that (see (21))

$$\frac{d}{da} e^{az} Je_0(a, z) = e^{az} \left\{ zJe_0(a, z) - \int_0^z e^{-at} t J_0(t)\, dt \right\}. \quad (61)$$

We have previously shown that the second integral on the right-hand-side of this equation can be rewritten in terms of $Je_0(a, z)$ (see (55) and (57)); therefore, (61) can be written as

$$\frac{d}{da} e^{az} Je_0(a, z) = \left[z - \frac{a}{(a^2+1)} \right] e^{az} Je_0(a, z) + \frac{z}{(a^2+1)} [aJ_0(z) - J_1(z)]. \quad (62)$$

Now, using the results in Table III, (47), (59), (60), and (62), we find that

$$\mathcal{I}_5(\lambda, x, y, P) = \left(\frac{P}{P^2-1} \right) [\mathcal{I}_7(\lambda, x, y, 0, P) + \mathcal{I}_8(\lambda, x, y, 0, P)] + \mathcal{I}_{10}(\lambda, x, y, P) + \mathcal{I}_{11}(\lambda, x, y, P); \qquad P > 1, \quad (63)$$

where $\mathcal{I}_{10}$ is defined in Table III and

$$\mathcal{I}_{11}(\lambda, x, y, P) = -\frac{\pi\lambda r}{(P^2-1)} \{ \sqrt{1-F_+^2}\, e^{-j\lambda F_+ r} + \sqrt{1-F_-^2}\, e^{-j\lambda F_- r} \}. \quad (64)$$

Using the same argument as before, we can neglect $\mathcal{I}_8$ when we derive the expression for $\hat{\mathcal{I}}_3$. Likewise, since

$$(2 + 4\cos^2(k_A d))\, \mathcal{I}_{11}(\lambda, x, y, P) - 4\cos(k_A d) \times [\mathcal{I}_{11}(\lambda, x+d, y, P) + \mathcal{I}_{11}(\lambda, x-d, y, P)] + \mathcal{I}_{11}(\lambda, x+2d, y, P) + \mathcal{I}_{11}(\lambda, x-2d, y, P)] = 0, \quad (65)$$

when $S_4 = 1$ and $P = k_A/\lambda$, we can also neglect $\mathcal{I}_{11}$ in the expression for $\hat{\mathcal{I}}_3$. Therefore, using (51) and (63), we obtain the expression for $\hat{\mathcal{I}}_3$ which is given in Table III. Now, if we use (19) and (20), where $\hat{\mathcal{I}}_3$ is used in place of $\mathcal{I}_3$, then we will obtain the correct result for $\mathcal{I}_1$ for the values of **S** in (26) and (27) when $0 \leqslant \lambda < k_A$. We have also listed the other important expressions which have been derived in this appendix in Table III.

A.5. $\hat{\mathcal{I}}_3$ *for* $\lambda > k_A$

The next step is to find an expression for $\hat{\mathcal{I}}_3$ that holds when $\lambda > k_A$ (i.e., $0 \leqslant P < 1$). As we have already mentioned, the integrand of (17) has a non-removable singularity when $\lambda > k_A$. On the other hand, the integral of interest, (8), only contains removable singularities for this case. Therefore, the contributions from the apparent singularities in (17) must cancel out when the desired integral, $\mathcal{I}_1$, is reconstructed

(see (19) and (20)). Since the contributions from the singularities all cancel out in the end, the method which is used to handle the singularities is unimportant, so long as the method is used consistently on each piece in the decomposition.

We found that analytic continuation arguments provided the simplest method for handling the case when $\lambda > k_A$. Earlier, we showed how $\mathscr{I}_1$ can be represented in terms of a finite number of ILHIs when $0 \leqslant \lambda < k_A$ (see (19), (20), and Table III). Since $\mathscr{I}_1$ and its expansion in terms of ILHIs are both analytic functions of λ for the values of **S** in (26) and (27), we can extend the region of validity for the previous results to $\lambda > k_A$ by letting

$$j\sqrt{P^2-1} = \sqrt{1-P^2}, \tag{66}$$

where $P = k_A/\lambda$. It should be pointed out that the complex conjugate operations in the expression for $\hat{\mathscr{I}}_3$ should be written out explicitly before (66) is applied. As it turns out, the expression for $\hat{\mathscr{I}}_3$, which is given in Table III, is still valid when $\lambda > k_A$.

A.6. *Reflection Properties for* $\hat{\mathscr{I}}_3$

Now that we have an expression for $\hat{\mathscr{I}}_3$, it is important to look at the reflection properties (i.e., reflections about $x = 0$ and $y = 0$) of this expression. Specifically, we would like to determine whether the relationships in (22) and (23) will still hold when $\hat{\mathscr{I}}_3$ is replaced by $\hat{\mathscr{I}}_3$. We will first look at $\hat{\mathscr{I}}_3(k_A, \lambda, x, -y, \mathbf{S})$. Referring to Table III, we find that

$$F_{\pm}(-\theta_0, P) = F_{\mp}(\theta_0, P). \tag{67}$$

Using the above relationship, it is easy to show that

$$\hat{\mathscr{I}}_3(k_A, \lambda, x, -y, \mathbf{S}) = (-1)^{S_1}\hat{\mathscr{I}}_3(k_A, \lambda, x, y, \mathbf{S}). \tag{68}$$

It is more difficult to handle $\hat{\mathscr{I}}_3(k_A, \lambda, -x, y, \mathbf{S})$, since we will need to handle the two cases $P > 1$ and $0 \leqslant P < 1$ separately. First, when $P > 1$ we find that

$$\begin{aligned} jF_{\pm}(\pi-\theta_0, P) &= [jF_{\pm}(\theta_0, P)]^* \\ \sqrt{1-F_{\pm}^2(\pi-\theta_0, P)} &= [\sqrt{1-F_{\pm}^2(\theta_0, P)}]^*. \end{aligned} \tag{69}$$

Substituting these results into Table III, we find that

$$\hat{\mathscr{I}}_3(k_A, \lambda, -x, y, \mathbf{S}) = (-1)^{S_2}\hat{\mathscr{I}}_3(k_A, \lambda, x, y, \mathbf{S}), \tag{70}$$

when $P > 1$. On the other hand, when $0 \leqslant P < 1$,

$$\begin{aligned} jF_{\pm}(\pi-\theta_0, P) &= [jF_{\mp}(\theta_0, P)]^* \\ \sqrt{1-F_{\pm}^2(\pi-\theta_0, P)} &= -\sqrt{1-F_{\mp}^2(\theta_0, P)}. \end{aligned} \tag{71}$$

Therefore, we can show that (70) still holds for this case.

A.7. *Definition of* $\hat{\hat{\mathscr{I}}}_3$

For the purposes of this appendix, we found that it was advantageous to neglect some of the terms in the expression for $\mathscr{I}_3$. In doing so, we obtained the expression for $\hat{\mathscr{I}}_3$. The expression for $\hat{\mathscr{I}}_3$ will be used throughout this paper, however, it is not always the most convenient expression to use.

Another expression can be obtained by reintroducing the terms that were neglected in the expression for $\hat{\mathscr{I}}_3$. These terms can be taken into account by defining the expression

$$\begin{aligned} &\hat{\hat{\mathscr{I}}}_3(k_A, \lambda, x, y, \mathbf{S}) \\ &\quad = D_1\{\mathscr{I}_7(\lambda, x, y, S_1, 1) + (-1)^{S_1-S_2} \\ &\qquad \times [\mathscr{I}_7(\lambda, x, y, S_1, 1)]^*\} \\ &\qquad + D_9\left\{\mathscr{I}_4\left(\lambda, x, y, S_1, \frac{k_A}{\lambda}\right) + (-1)^{S_1-S_2}\right. \\ &\qquad \left.\times\left[\mathscr{I}_4\left(\lambda, x, y, S_1, \frac{k_A}{\lambda}\right)\right]^*\right\} \\ &\qquad + D_5\left\{\mathscr{I}_{12}\left(\lambda, x, y, \frac{k_A}{\lambda}\right)\right. \\ &\qquad \left.+\left[\mathscr{I}_{12}\left(\lambda, x, y, \frac{k_A}{\lambda}\right)\right]^*\right\}, \end{aligned} \tag{72}$$

where an expression for $\mathscr{I}_4$ is given in (47) and

$$\begin{aligned} \mathscr{I}_{12}(\lambda, x, y, P) = \frac{\pi\lambda r}{(P^2-1)}\{&\sqrt{1-F_+^2}\, e^{-j\lambda F_+ r} \\ &\times [\sqrt{1-F_+^2}\, Je_0(-jF_+, \lambda r) - 1] \\ &+ \sqrt{1-F_-^2}\, e^{-j\lambda F_- r} \\ &\times [\sqrt{1-F_-^2}\, Je_0(-jF_-, \lambda r) - 1] \\ &- 2[J_1(\lambda r) - jP\cos\theta_0 J_0(\lambda r)]\}. \end{aligned} \tag{73}$$

Referring to (31), (47), and (63), we find that $\hat{\hat{\mathscr{I}}}_3 = \mathscr{I}_3$ when $P > 1$. However, $\hat{\hat{\mathscr{I}}}_3 \neq \mathscr{I}_3$ when $0 \leqslant P < 1$. The reason for this is discussed below. Since $\mathscr{I}_3$ (see (17)) is not an analytic function for values of $\lambda > k_A$, analytic continuation arguments can only be applied to $\mathscr{I}_1$, which in turn is composed of a number of pieces which have the form of $\mathscr{I}_3$ (see (19) and (20)). Therefore, even though $\hat{\hat{\mathscr{I}}}_3 \neq \mathscr{I}_3$ when $\lambda > k_A$, we can use $\hat{\hat{\mathscr{I}}}_3$ in place of $\mathscr{I}_3$ and still obtain the correct results for $\mathscr{I}_1$.

A.8. *Reflection Properties for* $\hat{\hat{\mathscr{I}}}_3$

As was the case with $\hat{\mathscr{I}}_3$, it is important to investigate the reflection properties of $\hat{\hat{\mathscr{I}}}_3$. If we apply (67) and (69) to (72), then we find that

$$\hat{\hat{\mathscr{I}}}_3(k_A, \lambda, x, -y, \mathbf{S}) = (-1)^{S_1}\hat{\hat{\mathscr{I}}}_3(k_A, \lambda, x, y, \mathbf{S}); \qquad \lambda \geq 0 \tag{74}$$

$$\hat{\hat{\mathscr{I}}}_3(k_A, \lambda, -x, y, \mathbf{S}) = (-1)^{S_2}\hat{\hat{\mathscr{I}}}_3(k_A, \lambda, x, y, \mathbf{S}); \qquad k_A > \lambda \geq 0. \tag{75}$$

These results are not surprising since we have previously shown that $\hat{\hat{\mathscr{I}}}_3 = \mathscr{I}_3$ when $k_A > \lambda \geq 0$ (see (22) and (23)).

When $\lambda > k_A$, we can use (71) to show that

$$\begin{aligned}\hat{\hat{\mathscr{I}}}_3(k_A, \lambda, -x, y, \mathbf{S}) &= (-1)^{S_2}\hat{\hat{\mathscr{I}}}_3(k_A, \lambda, x, y, \mathbf{S}) \\ &+ 2\pi j(\sqrt{1-P^2})^{S_1-1} D_9 \\ &\times \{(-1)^{S_1}[e^{j\lambda F_+ r} - (-1)^{S_1-S_2} e^{-j\lambda F_+ r}] \\ &+ e^{j\lambda F_- r} - (-1)^{S_1-S_2} e^{-j\lambda F_- r}\} \\ &+ \frac{2\pi\lambda r}{(P^2-1)} D_5\{\sqrt{1-F_+^2}\,[e^{j\lambda F_+ r} + e^{-j\lambda F_+ r}] \\ &+ \sqrt{1-F_-^2}\,[e^{j\lambda F_- r} + e^{-j\lambda F_- r}]\}. \end{aligned} \tag{76}$$

The fact that this result differs from (23) also should not be surprising, since we have previously shown that there is no reason for $\hat{\hat{\mathscr{I}}}_3$ to be equal to $\mathscr{I}_3$ when $\lambda > k_A$.

APPENDIX B: NUMERICAL COMPUTATION OF $\hat{\mathscr{I}}_3$

B.1. *Introduction*

In Appendix A, we demonstrated how $\hat{\mathscr{I}}_3$ can be written in terms of ILHIs, Bessel functions, and other elementary functions. In [36], it was shown that $Je_0(a, z)$ can be efficiently computed for all values of a and z, where $a \in \mathbb{C}$ and $z \in \Re$, by using either the Neumann series expansion [36, (58)], or one of the two factorial-Neumann series expansions [36, (29), (57)]. Actually, an algorithm was developed in [36] which uses these three expansions to compute a single ILHI, $Je_0(a, z)$, to a user-defined number of significant digits (SD). Now, in this appendix we will show how the ILHIs which appear in the decomposition of $\hat{\mathscr{I}}_3$ (see Table III) can be efficiently computed in parallel. We will make use of a number of the results from [36] in this appendix. It should be noted that a uniform asymptotic expansion for $Je_0(a, z)$ can also be obtained using the methods in [46].

The three expansions in [36, (29), (57), (58)] behave very differently for different values of the variables a and z. In [36], it is shown that the convergent factorial-Neumann series expansion converges most rapidly for small to moderate values of $z\,|\sqrt{a^2+1}|$. On the other hand, the asymptotic factorial-Neumann series expansion can be used when $z\,|a^2+1|$ is large. Finally, the Neumann series expansion fills in the gap left by the other two expansions, since it is most useful when $|\sqrt{a^2+1}+a| \geq 1$ and z has a small to moderate value.

B.2. *Computation of the ILHIs for* $0 \leq \lambda < k_A$

We will first handle the case when $\lambda < k_A$. For the applications in this paper, $r(x, y)$ will have a maximum value of a few wavelengths; therefore, $z = \lambda r$ will have a small to moderate value when $\lambda < k_A$. Since z is relatively small when $\lambda < k_A$, we will use the backward recurrence algorithm which was outlined in Section 6 of [36] to compute the sequence of Bessel functions.

In order to evaluate $\mathscr{I}_7(\lambda, x, y, S_1, 1)$, we must compute (see Table III)

$$Je_0(j\cos\theta_0, \lambda r). \tag{77}$$

For this ILHI, we find that

$$|a^2+1| = \sin^2\theta_0 \leq 1; \tag{78}$$

therefore, the convergent factorial-Neumann series expansion is the best expansion to use for the computation of (77). When we are computing the elements in the impedance matrix, it is possible to save some computation time because we only need to compute the real part of $\mathscr{I}_7(\lambda, x, y, 0, 1)$ (see (26) and Table III). Therefore, it can be shown that

$$\begin{aligned}\Re\{\mathscr{I}_7(\lambda, x, y, 0, 1)\} &= 2\pi\lambda\left\{rJ_1(\lambda r) - \lambda y^2\Gamma\left(\frac{3}{2}\right)\right. \\ &\left.\times \sum_{k=0}^{\infty}\left[\frac{\lambda y^2}{2r}\right]^k \frac{J_k(\lambda r)}{\Gamma(k+3/2)}\right\}; \qquad S_4 = 1. \end{aligned} \tag{79}$$

On the other hand, if we are interested in computing the electric field, then we will have to use

$$\begin{aligned}\mathscr{I}_7(\lambda, x, y, 1, 1) &= -2\pi j\lambda y\Gamma\left(\frac{3}{2}\right)\sum_{k=0}^{\infty}\left[\frac{\lambda y^2}{2r}\right]^k \\ &\times \frac{[J_k(\lambda r) + j\cos\theta_0 J_{k+1}(\lambda r)]}{\Gamma(k+3/2)}; \qquad S_4 = 0. \end{aligned} \tag{80}$$

We only need to compute $\mathscr{I}_7(\lambda, x, y, S_1, 1)$ for $S_1 = 1$, since $D_1 = 0$ when $\mathbf{S} = (0, 1, 0, 0)$ (see (27) and Table III).

The only other ILHIs that need to be computed in order to evaluate $\mathscr{I}_3$ are

$$\begin{aligned} &Je_0(-jF_+, \lambda r) \\ &Je_0(-jF_-, \lambda r). \end{aligned} \tag{81}$$

If we refer to Table III, we find that the factor

$$|a^2+1| = |1-F_{\pm}^2| = P^2 - \cos^2\theta_0 \tag{82}$$

may be much greater than one when $P = k_A/\lambda > 1$. Therefore, the convergent factorial-Neumann series expansion will not provide the most efficient method for the computation of the ILHIs in (81). On the other hand, we can show that

$$\begin{aligned} a+\sqrt{a^2+1} &= -jF_{\pm} + \sqrt{1-F_{\pm}^2} \\ &= \frac{j}{\lambda} e^{\mp j\theta_0}[k_A + \sqrt{k_A^2-\lambda^2}]. \end{aligned} \tag{83}$$

Since $|a+\sqrt{a^2+1}| \geq 1$ when $\lambda < k_A$, we will use the Neumann series expansion to compute the ILHIs in (81).

At this point, it is convenient to define

$$\begin{aligned} &\mathscr{I}_{13}^{\pm}(\lambda, x, y, P) \\ &\quad = -e^{-j\lambda F_{\pm} r}[\sqrt{1-F_{\pm}^2}\, Je_0(-jF_{\pm}, \lambda r) - 1]. \end{aligned} \tag{84}$$

By using (83) and the Neumann series expansion, we find that $\mathscr{I}_{13}^{\pm}$ can be written as

$$\mathscr{I}_{13}^{\pm}(\lambda, x, y, P) = \sum_{k=0}^{\infty} \frac{(je^{\pm j\theta_0})^k \varepsilon_k J_k(\lambda r)}{[P+\sqrt{P^2-1}]^k}. \tag{85}$$

When $\lambda < k_A$, we find that it is convenient to use the expression for $\hat{\mathscr{I}}_3$ instead of the expression for $\mathscr{I}_3$. Therefore, using (84), we find that $\hat{\mathscr{I}}_3$ (see (72)) can be rewritten as

$$\begin{aligned} &\hat{\mathscr{I}}_3(k_A, \lambda, x, y, \mathbf{S}) \\ &\quad = D_1\{\mathscr{I}_7(\lambda, x, y, S_1, 1) + (-1)^{S_1-S_2} \\ &\qquad \times [\mathscr{I}_7(\lambda, x, y, S_1, 1)]^*\} + D_9\pi j\left(\frac{j\sqrt{k_A^2-\lambda^2}}{\lambda}\right)^{S_1-1} \\ &\qquad \times \left\{\mathscr{I}_{13}^{+}\left(\lambda, x, y, \frac{k_A}{\lambda}\right) + (-1)^{S_2} \right. \\ &\qquad \times \left[\mathscr{I}_{13}^{+}\left(\lambda, x, y, \frac{k_A}{\lambda}\right)\right]^* + (-1)^{S_1}\mathscr{I}_{13}^{-}\left(\lambda, x, y, \frac{k_A}{\lambda}\right) \\ &\qquad \left. + (-1)^{S_1-S_2}\left[\mathscr{I}_{13}^{-}\left(\lambda, x, y, \frac{k_A}{\lambda}\right)\right]^*\right\} \\ &\qquad - D_5\frac{2\pi\lambda^3 r}{k_A^2-\lambda^2}\,\Re\left\{\sqrt{1-F_+^2}\,\mathscr{I}_{13}^{+}\left(\lambda, x, y, \frac{k_A}{\lambda}\right)\right. \\ &\qquad + \sqrt{1-F_-^2}\,\mathscr{I}_{13}^{-}\left(\lambda, x, y, \frac{k_A}{\lambda}\right) \\ &\qquad \left. + 2J_1(\lambda r)\right\}; \qquad 0 \leq \lambda < k_A, \end{aligned} \tag{86}$$

where (79) and (80) are used to compute $\mathscr{I}_7$, and (85) is used to compute $\mathscr{I}_{13}^{\pm}$.

As was shown in Appendix A, the expression for $\hat{\mathscr{I}}_3$ can be used in place of $\mathscr{I}_3$ in the expressions for $\mathscr{I}_1$. Also, the reflection equations for $\hat{\mathscr{I}}_3$ are given in (74) and (75).

B.3. *Computation of the ILHIs for $\lambda > k_A$*

Now we must handle the more difficult case when $\lambda > k_A$. Once again, we need to compute the integrals that are given in (77) and (81), but this time we need to use the definitions in Table III which are valid when $0 \leq P < 1$. For the integral in (77), the parameter $|a^2+1|$ will still behave as in (78). The expressions which were previously derived (see (79) and (80)) can still be used when $\lambda y^2/2r$ is small, but as the value of λ increases, more and more terms will be required in these expansions. Therefore, it is desirable to find a new way to compute (77) for large values of λ. Also, now that $\lambda > k_A$, the parameter $|a^2+1|$ will have a very different behavior for the two integrals given in (81). In fact, we now find that

$$\begin{aligned} |a^2+1| &= |1-F_{\pm}^2| \\ &= \cos^2\left(\theta_0 - \tan^{-1}\left(\frac{P}{\sqrt{1-P^2}}\right)\right) \leq 1; \\ &\qquad \lambda > k_A, \end{aligned} \tag{87}$$

where we have made use of (18). Once again, we will need to use a different method to compute the integrals in (81) now that $\lambda > k_A$. In this case, we need a way to determine which of the three expansions [36, (29), (57), (58)] will be best suited for the computation of $Je_0(a, z)$ for a given set of parameters, a, z, and SD. In order to accomplish this task, we will make use of some of the results which are given in [36].

For large values of λ, the argument of the Bessel functions (i.e., $z = \lambda r$), which are present in any of the expansions may become large. Therefore, it may be possible to use forward recurrence to obtain the desired sequence of Bessel functions. In order to use forward recurrence, we need to first obtain the starting functions $J_0(z)$ and $J_1(z)$. In [36], it was found that Hankel's asymptotic expansion can be used to obtain these starting functions whenever [36, (66)]

$$z > \mathrm{SD} + 4. \tag{88}$$

It may also be possible to use the asymptotic factorial-Neumann series expansion to compute $Je_0(a, z)$ when $z = \lambda r$ is large. We have previously shown in (78) and (87) that $|a^2+1| \leq 1$ for the integrals that we are interested in computing (i.e., (77) and (81)). Therefore, we find that [36, (72)],

$$z = \lambda r > k_{\max} = \frac{z\,|a^2+1| - 1}{2}. \tag{89}$$

Now, if we use the results in [36, (76), (77)], we find that the asymptotic factorial-Neumann series expansion can be used to compute $Je_0(a, z)$ to SD significant digits provided that

$$\frac{1}{2}\times 10^{-\mathrm{SD}}\,|e^{az}Je_0(a,z)| > \frac{2}{|a^2+1|\sqrt{\pi z}}\,e^{-z|a^2+1|/2}\max(1,|a|), \tag{90}$$

where the following approximation can be applied:

$$|e^{az}Je_0(a,z)| \sim \left|\frac{e^{az}}{\sqrt{a^2+1}}-\sqrt{\frac{2}{\pi z}}\,\frac{[a\cos(z-\pi/4)-\sin(z-\pi/4)]}{(a^2+1)}\right|; \quad \min(z, z\,|a\pm j|)\gg 0. \tag{91}$$

When $z > \mathrm{SD}+4$, but (90) is not satisfied, we still prefer to use forward recurrence to compute the sequence of Bessel functions; however, this time we would like to use the convergent factorial-Neumann series expansion to compute $Je_0(a, z)$. It can be shown that this method can be used if [36, (79)]

$$\frac{1}{2}\times 10^{-\mathrm{SD}}\,|e^{az}Je_0(a,z)| > \sqrt{\frac{z}{\pi}}\,\frac{e^{3/2}}{(2k_{\mathrm{int}}+3)}\left[\frac{ez\,|a^2+1|}{2k_{\mathrm{int}}+3}\right]^{k_{\mathrm{int}}}\max(1,|a|), \tag{92}$$

where

$$k_{\mathrm{int}} = \mathrm{int}(z). \tag{93}$$

When $z\,|a^2+1|\geq 2$, we can use the approximation for $|e^{az}Je_0(a, z)|$ which is given in (91). On the other hand, when $z\,|a^2+1|<2$, we can use [36, (80)]

$$|e^{az}Je_0(a,z)| \approx \sqrt{\frac{2z}{\pi}}\left|\cos\left(z-\frac{\pi}{4}\right)+a\cos\left(z-\frac{3\pi}{4}\right)\right|; \quad z\,|a^2+1|<2. \tag{94}$$

If the inequality in (88) is satisfied and if one out of the two inequalities in (90) or (92) are satisfied for each one of the integrals in (77) and (81), then we will use forward recurrence to compute the sequence of Bessel functions. If this is not the case, then a backward recurrence routine will have to be used to compute Bessel functions.

If neither of the inequalities in (90) or (92) are satisfied for a given integral (see (77) and (81)), then we will have to use backward recurrence to compute the Bessel functions, and we will have to find another way to compute that integral. Referring to [36, (29), (58)], we find that the convergent factorial-Neumann series expansion will converge faster than the Neumann series expansion when $z\,|a^2+1|\leq 2$. Therefore, we will use the convergent factorial-Neumann series expansion to compute $Je_0(a, z)$ when this is true. When $z\,|a^2+1|>2$ and $|a^2+1|\leq 1$, the convergent factorial-Neumann series expansion will still converge faster than the Neumann series expansion, but now we need to worry about round-off errors. In Section 6 of [36], it is shown that in order to use the convergent factorial-Neumann series expansion to compute $Je_0(a, z)$ to SD significant digits when $z\,|a^2+1|>2$ and $|a^2+1|\leq 1$, all operations have to be carried out to SDN significant digits, where

$$\mathrm{SDN} = \mathrm{SD} - \log_{10}\left(\frac{|a^2+1|\sqrt{\pi z}\,e^{z[\Re(a)-|a^2+1|/2]}}{\max(1,|a|)}\right). \tag{95}$$

Therefore, if the computer has at least SDN significant digits of accuracy, then the convergent factorial-Neumann series can be used to compute $Je_0(a, z)$. If the convergent factorial-Neumann series expansion is used for this case, then we will also have to calculate the sequence of Bessel functions to SDN, instead of SD, significant digits.

Finally, if the parameters a, z, and SD are such that none of the previously mentioned methods can be used, then we will use backward recurrence to compute the sequence of Bessel functions, and the Neumann series expansion [36, (58)] will be used to calculate $Je_0(a, z)$. An algorithm which is structured as outlined in this appendix can be used to compute the ILHIs which are encountered in the expression for $\hat{\mathcal{I}}_3(k_A, \lambda, x, y, \mathbf{S})$.

REFERENCES

1. A. Sommerfeld, *Ann. Phys.* (4th Folge) **28**, 665 (1909).
2. H. von Hörschelman, Dissertation, Munich; *Jahrb. drahtl. Telegra. Teleph.* **5**, 14, 188 (1911).
3. G. J. Elias, *Physica* **2**, 207, 361 (1922).
4. A. Sommerfeld, *Ann. Phys.* (4th Folge) **81**, 1135 (1926).
5. A. Baños, Jr., *Dipole Radiation in the Presence of a Conducting Half-Space* (Pergamon, Oxford, 1966).
6. J. R. Wait, *Electromagnetic Waves in Stratified Media* (Pergamon, Oxford, 1970).
7. G. Tyras, *Radiation and Propagation of Electromagnetic Waves* (Academic Press, New York, 1969).
8. W. C. Kuo and K. K. Mei, *Radio Sci.* **13**, 407 (1978).
9. E. F. Kuester and D. C. Chang, Scientific Report No. 43, Electromagnetics Lab., Department of Electrical Engrg., University of Colorado, Boulder, CO 80309, 1979 (unpublished).
10. H. A. Haddad and D. C. Chang, Scientific Report No. 22, Electromagnetics Lab., Department of Electrical Engrg., University of Colorado, Boulder, CO 80309, 1977 (unpublished).

11. J. J. H. Wang, *Proc. Inst. Elec. Eng.* **132**, Pt. H, 58 (1985).
12. T. Sphicopoulos, V. Teodoridis, and F. E. Gardiol, *Proc. Inst. Elec. Eng.* **132**, Pt. H, 329 (1985).
13. N. K. Das and D. M. Pozar, *IEEE Trans. Microwave Theory Tech.* **MTT-35**, 326 (1987).
14. L. Beyne and D. De Zutter, *IEEE Trans. Microwave Theory Tech.* **MTT-36**, 875 (1988).
15. D. M. Pozar, *IEEE Trans. Antennas Propag.* **AP-30**, 1191 (1982).
16. M. C. Bailey and M. D. Deshpande, *IEEE Trans. Antennas Propag.* **AP-30**, 651 (1982).
17. J. R. Mosig and F. E. Gardiol, *Advances in Electronics and Electron Physics*, Vol. 59, (Academic Press, New York, 1982), p. 139.
18. E. H. Newman, J. H. Richmond, and B. W. Kwan, *IEEE Trans. Microwave Theory Tech.* **MTT-31**, 941 (1983).
19. J. R. Mosig and F. E. Gardiol, *Proc. Inst. Elec. Eng.* **132**, Pt. H, 424 (1985).
20. K. A. Michalski, *Arch. Elektron. Übertragungstech.* **39**, 317 (1985).
21. R. H. Jansen, *IEEE Trans. Microwave Theory Tech.* **MTT-33**, 1043 (1985).
22. R. F. Harrington, *Field Computation by Moment Methods* (Krieger, Melbourne, FL, 1968).
23. S. L. Dvorak and E. F. Kuester, Scientific Report No. 94, Electromagnetics Lab., Department of Electrical Engrg. University of Colorado, Boulder, CO 80309, 1989 (unpublished).
24. J. R. Mosig and F. E. Gardiol, *IEEE AP-S Int. Symp.*, 379 (1979).
25. G. J. Burke, E. K. Miller, J. N. Brittingham, D. L. Lager, R. J. Lytle, and J. T. Okada, Report UCID-18626, Lawrence Livermore Lab., University of California, Livermore, CA, 1980 (unpublished).
26. I. E. Rana and N. G. Alexópoulos, *IEEE Trans. Antennas Propag.* **AP-29**, 99 (1981).
27. J. R. Mosig and F. E. Gardiol, *Proc. Inst. Elec. Eng.* **130**, Pt. H, 175 (1983).
28. P. B. Katehi and N. G. Alexópoulos, *J. Math. Phys.* **24**, 527 (1983).
29. D. R. Jackson and N. G. Alexópoulos, *IEEE Trans. Antennas Propag.* **AP-34**, 1467 (1986).
30. M. Marin, S. Barkeshli, and P. Pathak, *IEEE Trans. Microwave Theory Tech.* **MTT-37**, 669 (1989).
31. B. L. Brim, Ph.D. dissertation, Department of Electrical Engrg., University of Colorado, Boulder, CO 80309, in preparation.
32. N. K. Uzunoglu, N. G. Alexópoulos, and J. G. Fikioris, *IEEE Trans. Antennas Propag.* **AP-27**, 853 (1979).
33. D. M. Pozar, *Electromagn.* **3**, 299 (1983).
34. M. Kominami and K. Rokushima, *Denshi Tsushin Gakkai Ronbunshi B* **69**, 941 (1986) [Japanese]; *Electron. Commun. Jpn*, Part 1, **71**, No. 2, 113 (1988).
35. S. L. Dvorak and E. F. Kuester, *J. Comput. Phys.* **98**, 217 (1992).
36. S. L. Dvorak and E. F. Kuester, *J. Comput. Phys.* **87**, No. 2, 301 (1990).
37. S. L. Dvorak, Ph.D. dissertation, Department of Electrical Engrg., University of Colorado, Boulder, CO 80309, 1989 (unpublished).
38. D. M. Pozar, *IEEE Trans. Antennas Propag.* **AP-33**, 1045 (1985).
39. D. M. Pozar, *IEEE Trans. Antennas Propag.* **AP-34**, 658 (1986).
40. M. D. Deshpande and M. C. Bailey, *IEEE Trans. Antennas Propag.* **AP-30**, 645 (1982).
41. P. B. Katehi and N. G. Alexópoulos, *IEEE Trans. Antennas Propag.* **AP-31**, 34 (1983).
42. *The NAG Fortran Mini Manual, Mark 12*, (Numerical Algorithms Group Ltd., Oxford, UK, 1977).
43. W. H. Press, B. P. Flannery, S. A. Teukolsky, and W. T. Vetterling, *Numerical Recipes—The Art of Scientific Computing* (Cambridge Univ. Press, Cambridge, UK, 1986).
44. L. Beyne and D. De Zutter, *IEEE Trans. Microwave Theory Tech.* **MTT-36**, 126 (1988).
45. S. L. Dvorak and E. F. Kuester, *Int. J. Micro. Millimeter-Wave Computer-Aided Eng.* **4**, 333 (1991).
46. N. M. Temme, *SIAM J. Math. Anal.* **21**, 241 (1990).